Chemical Science

Accepted Manuscript

This article can be cited before page numbers have been issued, to do this please use: Z. Liu, Q. Chao, J. Zhao, Y. Lin, P. Yu, M. Chen, S. Shi, Y. Xiang, J. Gao and Y. Ma, *Chem. Sci.*, 2026, DOI: 10.1039/D6SC04529D.

ROYAL SOCIETY OF CHEMISTRY

rsc.li/chemical-science

View Article Online
DOI: 10.1039/D6SC04529D

Substituent Engineering of Dynamic Covalent Bonds Enables Simultaneous Enhancement of Performance and Recyclability

Zhiyong Liu,[1,3]* Qian Chao,[3] Jinyan Zhao,[3] Ying Lin,[3] Ping Yu,[4] Min Chen,[5] Shengyu Shi,[3]* Yixin Xiang,[3] Jiangang Gao,[3] and Youwei Ma[2]*

1 School of Chemistry & Chemical Engineering, Anhui University, Hefei, China;

2 Institute of Materials, École Polytechnique Fédérale de Lausanne (EPFL), CH-1015 Lausanne, Switzerland;

3 School of Chemical and Environmental Engineering, Anhui Polytechnic University, Wuhu, China;

4 School of Environmental and Chemical Engineering, Jiangsu Ocean University, Lianyungang, China;

5 Center for Water and Ecology, State Key Joint Laboratory of Environment Simulation and Pollution Control, School of Environment, Tsinghua University, Beijing, China.

* Correspondance Z. Liu: liuzhiyong@ahpu.edu.cn, S. Shi: shisy@ahpu.edu.cn, Y. Ma: youwei.ma@epfl.ch

Abstract

A central challenge in designing recyclable polymers lies in the trade-off between recyclability and performance. State-of-the-art strategies leveraging supramolecular interactions or dynamic covalent bonds (**DCB**s), either individually or in orthogonal combination, mostly end up improving one property with the compromise of the other. Here we present a unified molecular design strategy based on substituent engineering of **DCB**s to simultaneously enhance service-life performance and end-of-life recyclability. By introducing a β-ketoester substituent into dynamic oxime–urethane (**OU**) linkages, intermolecular hydrogen bonding is strengthened while bond thermodynamics are biased toward dissociation. We show that the engineered poly(**OU**)s exhibits improved mechanical and thermomechanical properties (e.g., 38 *vs* 24 MPa in tensile strength; 360 *vs* 169 MPa in Young's

modulus; 36 *vs* 20 ℃ in T_g) compared to the control sample lacking the β-ketoester moieties. Meanwhile, efficient depolymerization is achieved under mild conditions (140 °C), enabling recovery of the constituent components in high yields via simple vacuum distillation, particularly with the isocyanate yield of 87%, in contrast to only 14% for the depolymerization of normal poly(**OU**). The materials are also thermally reprocessable and enable closed-loop recycling of carbon fiber-reinforced composites. This work establishes substituent engineering of **DCB**s as a general strategy to decouple recyclability and performance, offering a pathway toward high-performance circular polymer materials.

Introduction

The replacement of petroleum-derived plastics with recyclable polymers represents one of the pillars of a transition toward a circular economy.[1–3] However, the development of such materials is fundamentally constrained by a long-standing trade-off between recyclability and performance.[4–6] High performance requires stable, strongly interconnected networks that restrict chain mobility, whereas recyclability relies on bond reversibility and molecular mobility, thus making it challenging to optimize both simultaneously.[7] A representative example is that thermoplastics are intrinsically recyclable but often suffer from limited mechanical and thermal robustness, while cross-linking or filler reinforcement enhances performance at the expense of reprocessability.

State-of-the-art approaches to overcoming this dilemma consist in supramolecular engineering for thermoplastics[8–13] or the incorporation of dynamic covalent bonds (**DCB**s) as reversible cross-links in thermosets.[14–19] Supramolecular interactions (e.g., hydrogen bonding, metal–ligand coordination, and host–guest interactions) can reinforce thermoplastics through reversible noncovalent bonding, yet to an extent reduce their recyclability due to strengthened intermolecular associations.[20,21] In contrast, the recently extensively investigated **DCB**s includes disulfide bonds,[22–24] cyanurate,[25–27] tri/di-ketoenamines,[6,28–30] vinylogous urethanes,[31–35] dioxaborolanes,[16,36–38] to name a few, enabling reprocessability and chemical recycling of thermosets via bond exchange or dissociation. They sometimes compromise thermal and mechanical properties of the materials owing to the intrinsic lability of these reversible linkages.[39] Although the combined use of supramolecular interactions with

View Article Online
DOI: 10.1039/D6SC04529D

DCBs has emerged as a promising strategy,[40–43] these elements are typically introduced in an orthogonal manner, and also end up trading one property off the other.

This dilemma is particularly evident in polyurethane and polyurea fields. Incorporation of supramolecular interactions into linear or branched polyurethanes and polyureas can significantly enhance mechanical strength, thermal stability, and chemical resistance;[13,44,45] however, the resulting materials often require harsher conditions for recycling or reprocessing, such as elevated temperatures, the presence of (more) catalysts, or excess depolymerization agents. In parallel, replacing conventional urethane or urea linkages with isocyanate-derived **DCB**s such as hindered urea,[46] pyrazole–urea,[47] and oxime–urethane linkages,[48] confers intrinsic recyclability and reprocessability to cross-linked networks, but sometimes at the expense of thermal and mechanical performance. Subsequent efforts to incorporate supramolecular interactions into these dynamic covalent networks (with no chemical alteration to DCBs) can improve material performance,[49,50] yet typically lead to more demanding recycling conditions. Moreover, despite nearly a century of development in isocyanate-based polymer chemistry, direct recycling of isocyanates from their derived polymers remains exceedingly rare due to their high reactivity and propensity for side reactions.[51]

To challenge the status quo, here we propose a general molecular design strategy based on substituent engineering of **DCB**s. Unlike the orthogonal use of **DCB**s and supramolecular bonds, this strategy involves simultaneous modulation of intermolecular interactions and bond thermodynamics at the same reactive site. Specifically, we selected the well-established oxime–urethane (**OU**) bonds as the model system.[48,52–56] They are functionalized with a β-ketoester motif, an essential synthon that was introduced by the Du Prez lab to the realm of recyclable polymer synthesis,[31,33,34,57] and subsequently attracted extensive investigations, including the research from some of our authors.[35,58–61] The functionalization serves a dual and cooperative role (Scheme 1): the additional carbonyl groups enhance intermolecular hydrogen bonding,[58,62] thereby improving thermal and mechanical properties, while the electron-withdrawing nature of the β-ketoester lowers the thermodynamic stability of the **OU** linkage, shifting the equilibrium toward dissociation.[63,64] This dual-function design enables the resulting poly(acetoacetated oxime–urethane)s (**PAOU**s) to achieve both enhanced service-life performance and

View Article Online
DOI: 10.1039/D6SC04529D

efficient end-of-life recyclability. The **PAOU**s exhibit improved mechanical and thermomechanical properties compared to the poly(**OU**) lacking the β-ketoester moiety (Scheme 1b). Small-molecule model studies and mechanistic investigations demonstrate that the acetoacetated oxime–urethane (**AOU**) bonds exhibit a significantly reduced equilibrium constant, favoring dissociation into isocyanates and acetoacetated oximes at equilibrium (Scheme 1a). Consequently, **PAOU**s can be depolymerized under mild conditions (140 °C), enabling high-yield recovery of monomers via simple vacuum distillation. Notably, isocyanates are recovered in up to 87% yield—a rarely reported achievement due to the high reactivity of isocyanates—whereas the poly(**OU**) control exhibits minimal recovery (<14%).

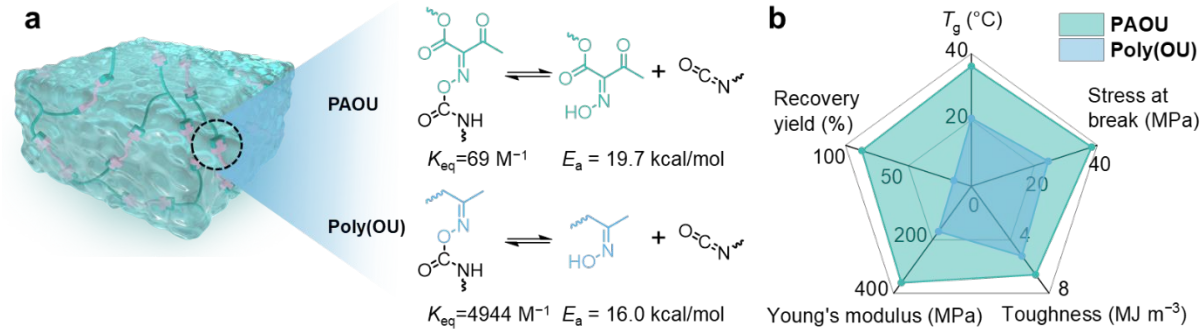

Scheme 1. (a) Comparison of the activation energy E_a and reaction equilibrium constant K_{eq} for the reversible reactions of **AOU** and **OU** bonds. (b) Radar map to compare the key performance matrixes and the recycling efficiency of **PAOU** and poly(**OU**) networks.

Results and Discussion

Synthesis and Characterizations of PAOUs, and the Comparison with a Normal Poly(OU)

The synthesis of **PAOU**s starts from a two-step modification (including acetoacetylation and oximation reactions; details seen in SI) to convert trimethylolpropane into trimethylolpropane acetoacetate oximes (**TAO**), followed by the cross-linking of **TAO** with three different di-isocyanates including TMDI, HDI, and HMDI to produce the corresponding **PAOU-TMDI**, **PAOU-HDI**, and **PAOU-HMDI** networks (Figure 1a). FTIR analysis shows that the emergence of a new peak at 1520 cm^{-1} attributed to

View Article Online
DOI: 10.1039/D6SC04529D

the stretching vibration of C–N in the urethane moiety, together with the shift of the ester carbonyl (C=O) stretching vibration from 1747 to 1761 cm^{-1}, supports the successful formation of **AOU** linkages (Figure 1b). The materials exhibit excellent chemical resistance, as reflected by non-dissolution of the **PAOU-HDI** films when immersed in various organic solvents including 1,4-dioxane, THF, toluene, and $CHCl_3$ for 7 days (Figure 1c). Moreover, the three **PAOU**s networks display swelling ratios of 40–170% (Figure S1), and regardless of the solvent type, their gel fractions are comparable, all around 90% (Figure 1d), indicating the same level of cross-link densities present in them.

Differential Scanning Calorimetry (DSC) analysis reveals that all **PAOU** networks exhibit a glass transition temperature (T_g) ranging between 22 ℃ to 44 ℃ (Figure 1e). Among them, **PAOU-HMDI** possesses the highest T_g, which primarily arises from the rigid 4,4-methylenedicyclohexyl skeleton brought by HMDI. Dynamic Mechanical Analysis (DMA) traces show a sharp drop in storage modulus *E*', along with the emergence of a peak in the tan δ plots at the temperature of 31–57 ℃ (Figure 1f), which marks their T_g. The T_g thus measured follows the same trend as those obtained from DSC (Figure 1e), but differ by ca. 10 ℃ in the specific value. This discrepancy is primarily attributed to the 1 Hz of oscillating force employed in the DMA measurement, consistent with previous reports.[65,66] Following the thermal transition, a rubbery regime appears in all **PAOU** films, and the *E*' values of the rubbery plateau converge to approximately 4.5 MPa for all samples (Figure 1f), reaffirming their comparable cross-link densities.

The stress–strain curves of all three **PAOU**s display plastic-like tensile behavior, with the stress at break of 32–64 MPa and the strain at break of 7–63% (Figure 1g). Among them, **PAOU-TMDI** and **PAOU-HMDI** outperform their counterparts in terms of extensibility and rigidity, respectively. More specifically, upon varying the diisocyanate cross-linker from **TMDI** to **HDI** and **HMDI**, it leads to a progressive increase in stress at break while a decrease in strain at break (Figure 1g). This is mainly because of the increased T_g that restricts polymer chain mobility and thereby enhances stiffness at the expense of extensibility (Figure 1e).

Systematic comparisons of **PAOU-HDI** and a poly(**OU**) sample (lacking the β-ketoester substituent; synthesis details seen in SI) in thermal, thermomechanical, and mechanical properties were made; As

View Article Online
DOI: 10.1039/D6SC04529D

shown in Figures 1e–g, they demonstrate that the **PAOU-HDI** shows higher stress at break (38 *vs* 24 MPa), Young's modulus (360 *vs* 169 MPa), and toughness (6.6 vs 5.3 MJ m^{-3}), and higher *T*g determined by both DSC (36 *vs* 20 ℃) and DMA (41 *vs* 37 ℃) than those of the poly(**OU**) control. The performance enhancement is first because the presence of two carbonyl groups in **AOU** serves as hydrogen-bonding acceptors to urethane amine proton.[58,62] We then employed Density Functional Theory (DFT) calculations (M06-2X/def2-TZVP) to investigate the hydrogen bonding interactions. It shows that the hydrogen bond between two **AOU**s exhibits a higher calculated intensity of 2.2 kcal/mol as compared to only 1.8 kcal/mol present in two normal **OU**s (Figure S2). Thus, the increased number and intensity of hydrogen-bonds jointly strengthen the polymer networks.

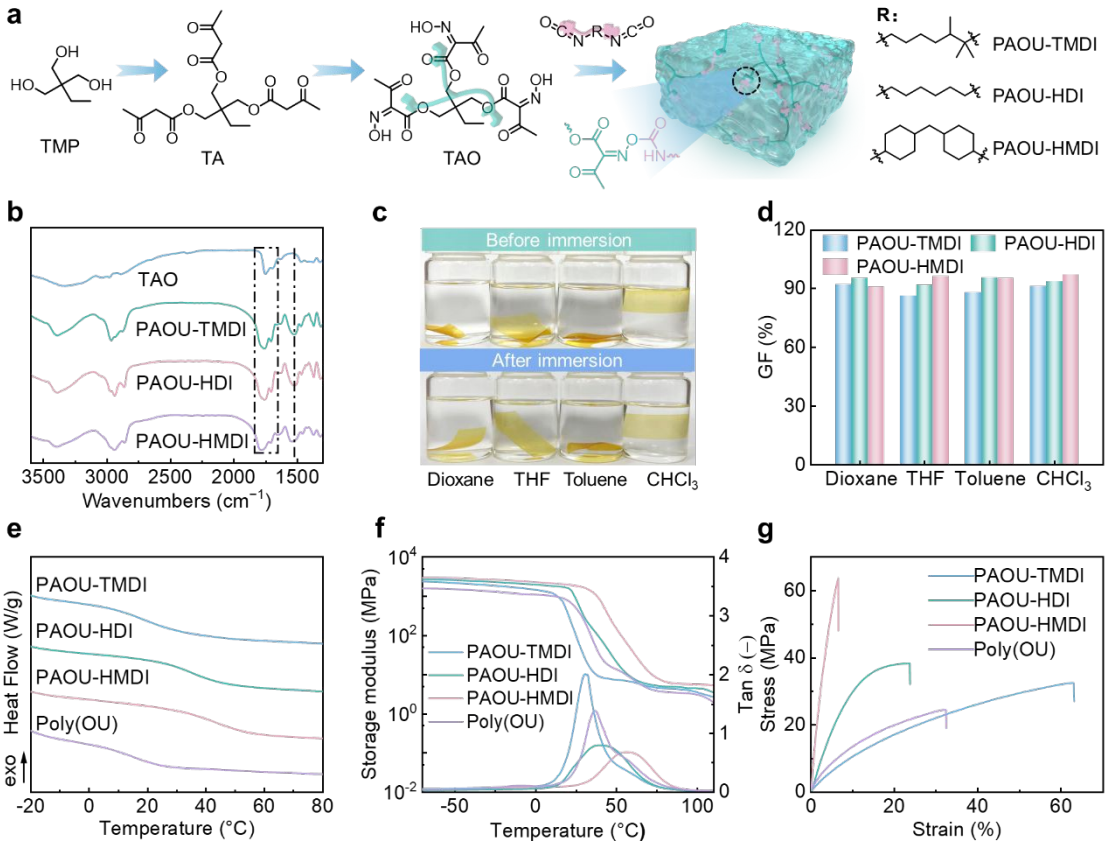

Figure 1. (a) Synthesis of **PAOU**s through the polymerization of **TAO** and three types of isocyanates (TMDI, HDI, and HMDI). (b) FTIR spectra of **TAO** and **PAOU**s. (c) Photographs of **PAOU-HDI** films dispersed in various solvents at room temperature before and after 7 days. (d) Gel fraction, (e) DSC traces, (f) DMA traces, and (g) stress–strain curves of **PAOU**s, and a poly(**OU**) synthesized through the polymerization of a normal trifunctional oxime and HDI.

View Article Online
DOI: 10.1039/D6SC04529D

Reprocessing and Chemical Recycling of Poly(OU)s and their Composites

Having confirmed the reinforcing role of the β-ketoester substituent on **PAOU** networks, we next investigated its impact on chemical recyclability. Existing strategies for chemically recycling polyurethanes and their analogues primarily rely on catalytic activation of urethane exchange or dissociation reactions,[67–69] or on the incorporation of isocyanate-derived **DCB**s.[46–48,53,58,70] The recycling processes often proceed in the presence of a large excess of nucleophililes (e.g., amines or alcohols) to selectively break the isocyanate-derived bonds upon thermal treatment. The nucleophilic substitution-induced depolymerization indeed allows to recover the constituent nucleophilic components of polyurethanes and their analogues, but converts isocyanate units into (more stable) downstream derivatives (Table S1).[68,69,71–73] Since isocyanates account for a substantial fraction of the economic and environmental cost of polyurethanes, their direct recovery remains imperative.

The challenge of doing so arises from the high reactivity of isocyanates that can recombine with nucleophiles or undergo side reactions such as hydrolysis, biuret formation, and trimerization during depolymerization.[51] Here, we drew inspiration from reactive distillation strategies used for recovering reactive cyclic monomers via ring-closing depolymerization,[65,74] and adopted a vacuum distillation set-up to continuously separate the dissociated species. The depolymerization of **PAOU-HDI** was then carried out at a moderate temperature (140 °C) for 3 h under a reduced pressure of 0.01 Pa (Figures 2a, S3). Under these conditions, it enabled recovery of both **TAO** and HDI in high yields of 82% and 87%, respectively, with high chemical purity as confirmed by ^{1}H NMR spectroscopy (Figures 2b–c). The high quality of recovered materials was further supported, when we repolymerized them under the same conditions to the preparation of the parent **PAOU-HDI**, it refurnished the polymer networks of comparable thermomechanical and mechanical properties to the initial ones (Figures 2d–e). However, the same depolymerization treatment for the normal poly(**OU**) results in substantially lower recovery yields of oximes (11%) and HDI (14%). This marked difference highlights the significance of the β-ketoester substituent in improving the recycling efficiency of **PAOU**.

View Article Online
DOI: 10.1039/D6SC04529D

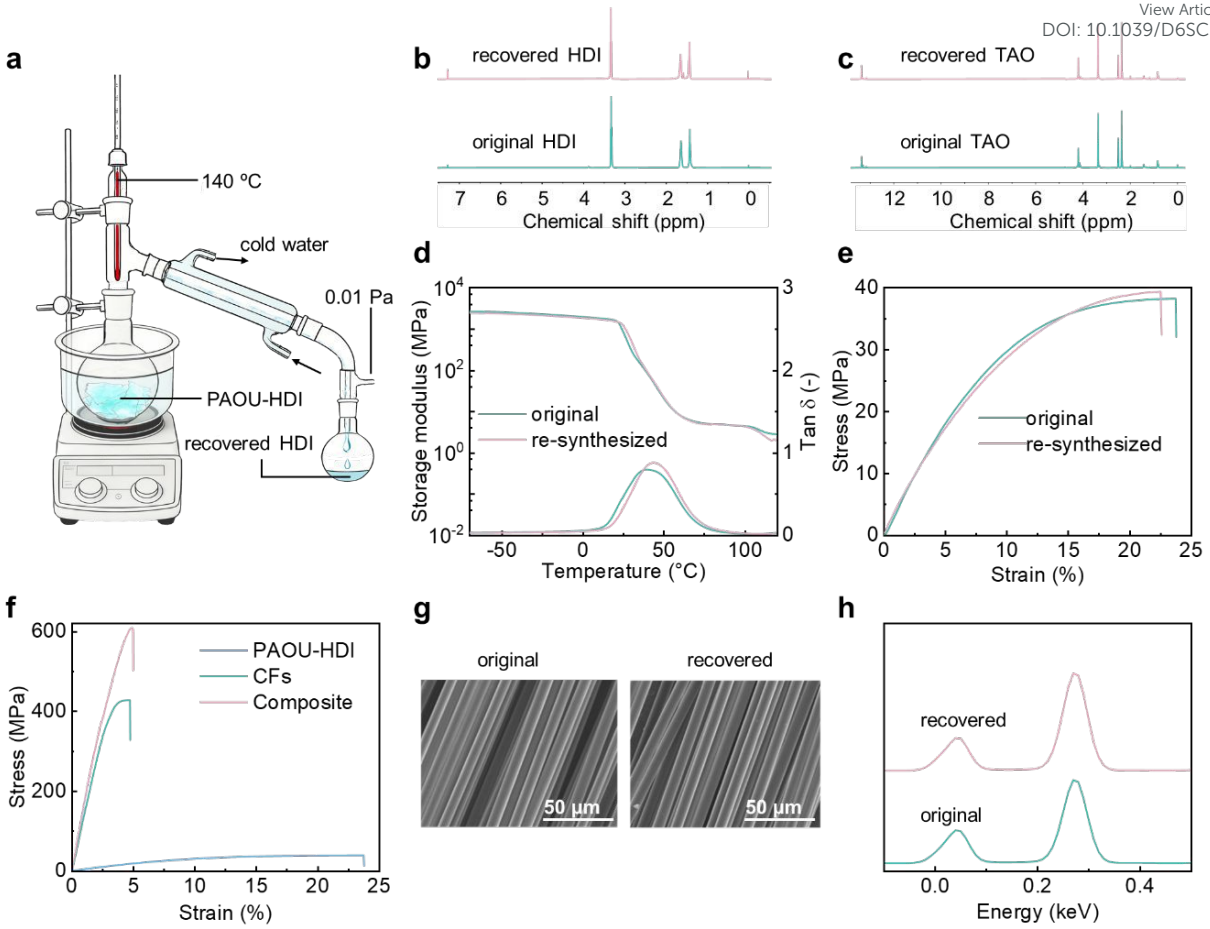

Figure 2. (a) Schematic illustration showing the simultaneous depolymerization of **PAOU-HDI** to separate both **TAO** and HDI by vacuum distillation. Comparison between the ^{1}H NMR spectra ($CDCl_3$, 400 MHz) of the original and recovered (b) HDI and (c) **TAO**. (d) DMA traces and (e) stress–strain curves of the original and re-synthesized **PAOU-HDI**. (f) Stress–strain curves of **PAOU-HDI**, CFs, and their composite. (g) SEM images and (h) EDX spectra of the original and recovered CFs.

The good performance and closed-loop recyclability of **PAOU**s potentially position them as attractive polymeric substrates for the fabrication of recyclable thermosetting composites. To confirm it, we endeavored to use **PAOU**s to prepare engineering materials through the composite with carbon fibers (CFs), which were subsequently subjected to chemical recycling analysis. The composite was fabricated by first impregnating CFs with the reaction mixture of **TAO** and **HDI**, followed by post-curing of the prepreg in a drying oven at 40 °C for 48 h. The resulting material exhibits significant improvement in

View Article Online
DOI: 10.1039/D6SC04529D

tensile strength to 607 MPa in comparison to 38 MPa of neat **PAOU-HDI** and 428 MPa of CFs (Figure 2f). Noteworthily, when we applied the vacuum distillation treatment on the composite, both **TAO** and **HDI** were afforded in high yields of 76% and 83%, respectively, and in high quality (Figures S4–S5). Effective recovery of the valuable CFs is also achieved; SEM (Figure 2g) and EDX (Figures 2h, S6–S7) analyses on the original and recycled CFs show that no distinguishable difference is noted, suggesting the good retainment of their morphology and chemical structure after the recycling.

Although chemical recycling is particularly advantageous for reusing CF-reinforced composites due to their non-flowable nature, thermal reprocessing remains a more energy- and resource-efficient approach.[75,76] Thus, we subsequently explored the reprocessability of **PAOU** networks. Their flowability, an essential parameter for assessing polymer reprocessability and determining feasible reprocessing conditions, was initially examined by stress relaxation experiments.[31,57] The results demonstrate that all three samples are capable of relaxing their stress in the temperature tested between 90–120 ℃, with the stress dissipated at a faster rate at higher temperature (Figure S8a–c). The increased stress relaxation rate primarily originates from the accelerated exchange reactions between **AOU**s at higher temperatures (Figure S9a), which enables the polymer networks to rearrange themselves more easily. Arrhenius analysis of the relaxation times yields E_a for stress relaxation that is comparable across all three **PAOU** networks, ranging from 36.8 to 38.5 kcal/mol (Figure S8d). This is a result of the same dynamic **AOU** bonds that serve as their network cross-links.

The stress–relaxation behavior guided us to reprocess the polymers by compression-molding at 100 °C under a pressure of 10 MPa for 0.5 h. The treatment refurnished homogeneous films even after being repeated three times, with the demonstration of the reprocessing of **PAOU-HDI** shown in Figure S9(b). FTIR analysis, DSC and tensile testing measurements were conducted on the reprocessed **PAOU**s, with the results compared with those of the original materials (Figures S9c–k). Gratifyingly, they exhibit no discernible differences before and after the reprocessing, confirming the excellent recovery of the chemical structures, thermal and mechanical properties, which describes the good reprocessability of the materials.

Investigation on the Mechanism of the Enhanced Recyclability of PAOU

View Article Online
DOI: 10.1039/D6SC04529D

The underlying mechanism for the improved recycling efficiency present in **PAOU** was first analyzed by small-molecule model studies. The experiments involved reacting either a normal **OU1** or an **AOU1** with an equimolar amount of phenethyl isocyanate (**2**) (Figures 3a–b). The reactions were conducted at 90–120 ℃, and monitored by ^{1}H NMR spectroscopy (Figures 3a–b, S10–S11). Under all conditions tested, both **AOU1** and **OU1** underwent efficient exchange to form the corresponding phenethyl-substituted analogues including **AOU2** and **OU2**, accompanied by the formation of butyl isocyanate (**1**) (Figures 3a–b). Kinetic analysis of the ^{1}H NMR signals determined the reaction rate constants k (Figures S10f, S11f). At 90 ℃, the k for the **AOU1-** and **OU1-**involved exchange reactions are 7.6×10^{-5} s^{-1} and 9.0×10^{-5} s^{-1}, respectively, which increase to 5.5×10^{-4} s^{-1} and 5.2×10^{-4} s^{-1} at 120 ℃, demonstrating the temperature dependence. Arrhenius analysis shows that the activation energies E_a for the reactions of **2** with **AOU1** and **OU1** are 19.7 or 16.0 kcal/mol, respectively (Figure 3c). The slightly higher E_a value present in the **2–AOU1** reaction suggests the presence of β-ketoester moiety in improving the kinetic stability of **AOU** bonds.

The impact of β-ketoester on thermodynamic equilibrium of the reactions was next investigated by reacting **1** with either an acetoacetated oxime (**AO**) or a normal oxime, namely 2-butanone oxime (**BO**), at room temperature for 48 h (Figures S12–S13). After the reaction, **BO** was converted to **OU** nearly quantitatively, whereas the conversion of **AO** to **AOU** reached ca. 82% independent of the initial stoichiometry (Figure S12; Tables S2–S3). Calculation of the reaction equilibrium constants K_{eq} shows that varying the amount of **1** relative to **AO** from 0.9 to 1.1 equiv. leads to a gradual decrease in K_{eq} from 111 to 51 M^{-1} (Figure 3d), probably due to competing side reactions involving isocyanates. Under stoichiometric conditions, the K_{eq} for **AOU** formation is nearly two orders of magnitude lower than that for the **OU**-forming reaction (69 *vs* 4944 M^{-1}). This reduced K_{eq} indicates that incorporation of the β-ketoester substituent shifts the equilibrium toward the dissociated state, thereby favoring the formation of free **AO**s and isocyanates.

View Article Online
DOI: 10.1039/D6SC04529D

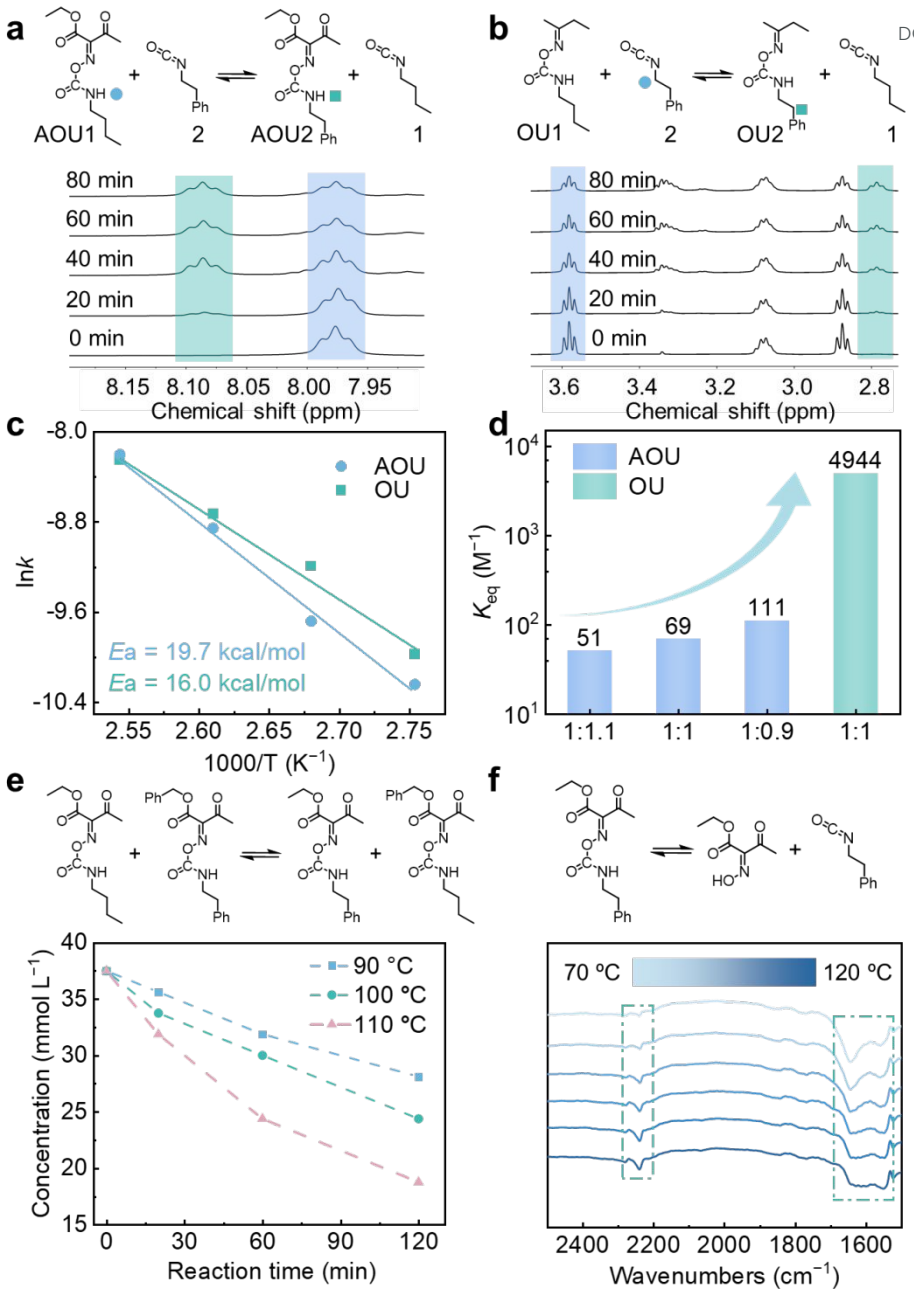

Figure 3. Exchange reaction between phenethyl isocyanate (**2**) and an equivalent amount of (a) **AOU1** or (b) **OU1** compound to form butyl isocyanate (**1**) and the corresponding **AOU2** or **OU2**, and the relevant ^{1}H NMR spectra recorded during these exchange reactions. (c) Arrhenius plots showing the logarithmic rate constants *k* for the conversion of **AOU1** and **OU1** into the corresponding **AOU2** and **OU2** as a function of inverse temperature. (d) K_{eq} for the reactions of **AO** and different equivalents of **1** or the reaction of **BO** and an equivalent amount of **1**. (e) Metathesis reaction between two **AOU** compounds, and the conversion variation for this reaction. (f) Thermal dissociation of a **AOU**

View Article Online
DOI: 10.1039/D6SC04529D

compound into an isocyanate and an **AO**, and the temperature-variable FTIR spectra of the **AOU** measured from 70 ℃ to 120 ℃, with an increment of 10 ℃.

We next explored the mechanism underlying the reversibility of **AOU** bonds. Given their structural similarity to normal **OU** bonds and Knoevenagel adducts, both of which are known to undergo thermally induced metathesis,[48,77–81] we anticipate that **AOU**s would exhibit similar associative exchange behavior (Figure 3e). To validate this, two **AOU** compounds were mixed in an equimolar ratio and heated at 90–110 ℃. Reaction progress was monitored by High-Performance Liquid Chromatography (HPLC), which confirms successful exchange between the two species, affording two additional **AOU** compounds (Figure S15). The reaction rate increases with temperature, indicating thermally accelerated exchange kinetics (Figure 3e). In parallel, the dissociative capability of **AOU** was assessed by temperature-variable FTIR spectroscopy. Upon heating from 70 ℃ to 120 ℃, the characteristic C=N stretching band at 1644 cm^{-1} progressively decreases and shifts to 1630 cm^{-1}, while the isocyanate absorption at 2240 cm^{-1} becomes increasingly pronounced (Figure 3f). These spectral changes provide clear evidence for thermal dissociation of **AOU** bonds into isocyanate and **AO** groups (Figure 3f). Taken together, these results demonstrate that **AOU** linkages can perform their reversibility through both associative and dissociative mechanisms (Figures 3e–f).

To further gain mechanistic insight, we then carried out DFT calculations (M06-2X/def2-TZVP) on the reactions of isocyanate **1** with **AO**, and also with **BO** as a control (Figure 4). Prior to nucleophilic addition to **1**, both **AO** and **BO** undergo isomerization to their corresponding nitrone tautomers (AO1 and BO1). For **AO**, this transformation proceeds via a unimolecular pathway facilitated by conjugation between the β-ketoester and oxime functionalities, which promotes intramolecular proton transfer (Figure S18). In contrast, such a pathway is energetically unfavorable for **BO** due to the absence of the β-ketoester substituent, as evidenced by the high calculated Gibbs free energy (ΔG^0) of 51.5 kcal/mol for the corresponding transition state BO-TS1 (Figure S19). Inspired by previous studies,[48,82] a bimolecular pathway was adopted, involving an initial association of two **BO** molecules to form a six-membered cyclic complex through intermolecular hydrogen bonding, followed by proton transfer

View Article Online
DOI: 10.1039/D6SC04529D

within the complex and subsequent dissociation into two BO1 species (Figure S20). This bimolecular isomerization route is chemically sound, with calculated ΔG^0 not exceeding 16.6 kcal/mol along the reaction coordinate.

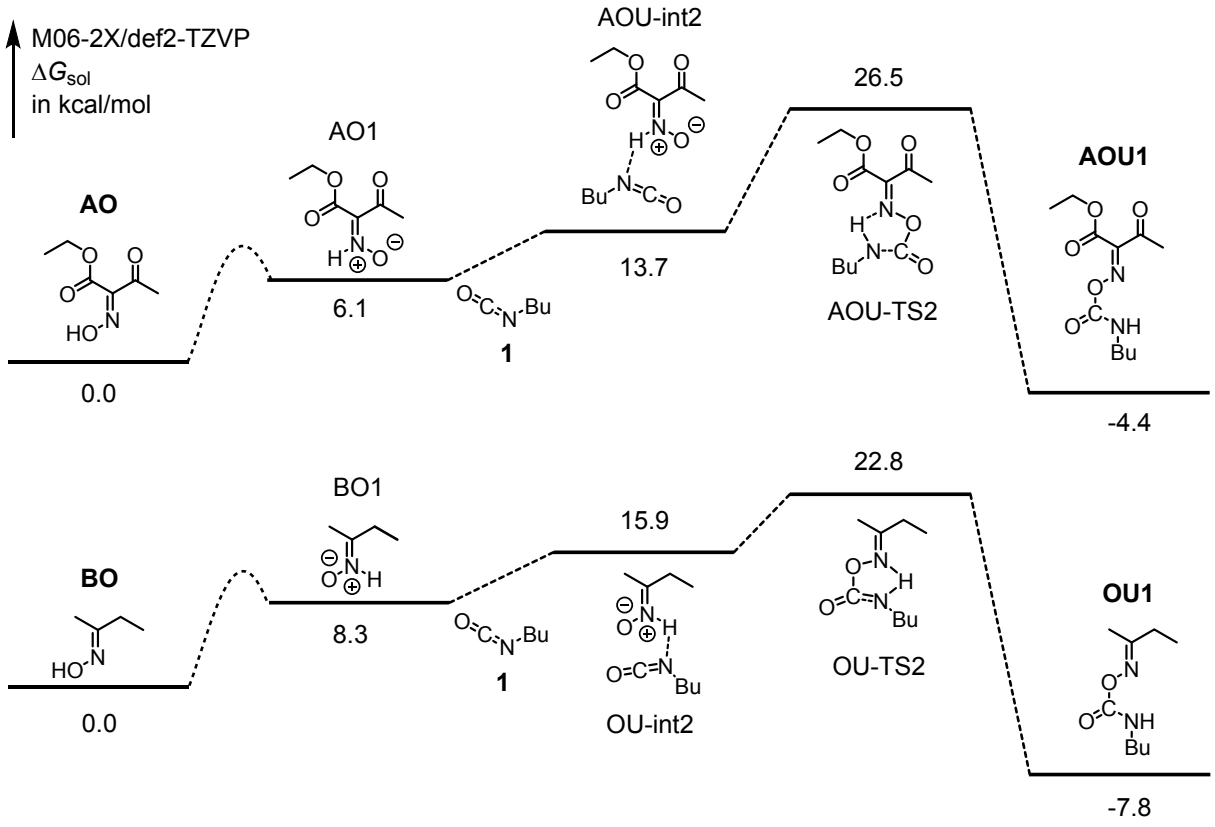

Figure 4. Gibbs free energies (ΔG^0) of the stationary points for the reaction of isocyanate **1** with **AO** (top) or **BO** (bottom) to form **AOU1** or **OU1**, respectively.

The nitrone intermediates AO1 and BO1 subsequently undergo nucleophilic addition to the isocyanate functionality, and afford the corresponding transition states AOU-TS2 and OU-TS2, with calculated ΔG^0 of 26.5 and 22.8 kcal/mol, respectively (Figure 4). These values correspond to the E_a for **AOU** and **OU** formation, indicating slightly lower kinetics in accessing **AOU**. This trend is consistent with experimental observations, where the reaction rate constant for affording **OU** is 6.3×10^{-5} s^{-1}, triple that (2.1×10^{-5} s^{-1}) for **AOU** formation (Figures S21). The calculated E_a for the reverse reactions are comparable for **AOU** and **OU** (30.9 *vs* 30.6 kcal/mol), suggesting similar kinetic accessibility for bond

View Article Online
DOI: 10.1039/D6SC04529D

cleavage. However, **AOU** exhibits a ΔG^0 of –4.4 kcal/mol, which is less negative than –7.8 kcal/mol of **OU**, substantiating its reduced thermodynamic stability and a greater propensity for dissociation.

Altogether, the combined experimental and computational results demonstrate that the β-ketoester substituent primarily modulates the thermodynamic landscape of the reversible reaction, favoring bond dissociation without significantly altering the kinetic barrier for cleavage. This shift in equilibrium increases the concentration of free **AO**s and isocyanates under reaction conditions. When coupled with vacuum-assisted distillation, this thermodynamic bias facilitates efficient separation and recovery of the dissociated species, thereby accounting for the enhanced recycling efficiency observed in **PAOU** networks.

Conclusion

In summary, this work demonstrates that substituent engineering of dynamic covalent bonds enables simultaneous control over intermolecular interactions and bond thermodynamics in recyclable polymers. Incorporation of a β-ketoester substituent into oxime–urethane linkages introduces additional hydrogen-bonding interactions that enhance network rigidity, resulting in improved mechanical and thermomechanical properties. At the same time, the substituent significantly shifts the thermodynamic equilibrium toward bond dissociation, as evidenced by a nearly two orders of magnitude reduction in equilibrium constant (69 *vs* 4944 M^{-1}). This thermodynamic bias enables efficient depolymerization at 140 °C, leading to high-yield recovery of acetoacetated oximes (82%) and isocyanates (87%) via vacuum distillation—an unprecedented achievement in polyurethane/polyurea chemistry. The dynamic networks further exhibit rapid stress relaxation, excellent reprocessability, and enable closed-loop recycling of carbon fiber–reinforced composites with preserved material integrity. Collectively, these findings establish substituent engineering as an effective strategy to decouple mechanical performance from recyclability by integrating supramolecular interactions and thermodynamic control within a single dynamic covalent bond.

Author contributions

View Article Online
DOI: 10.1039/D6SC04529D

Q. C. contributed methodology, investigation; J. Z. contributed investigation, software, methodology. Y. L., P. Y. contributed formal analysis; M. C., Y. X., and J. G. contributed investigation, testing, and analysis; S. S.: Small-molecule synthesis and analysis; Y. M. and Z. L.: contributed funding acquisition, conceptualization, methodology supervision, writing– original draft, reviewing and editing.

Conflicts of interest

There are no conflicts to declare.

Data availability

The data supporting this article have been included as part of the supplementary information (SI). Supplementary information: materials, experimental procedures, characterizations, theoretical calculations, SI Figure S1–S45. See DOI: XXXX.

Acknowledgements

Z.L. and S.S. thank the support from the National Natural Science Foundation of China (grant no. 52403151 and 52503001) and the Natural Science Foundation of Anhui Province (grant no. 2108085QE200).

References

1 Y. Zhu, C. Romain and C. K. Williams, *Nature*, 2016, **540**, 354–362.
2 P. Shieh, W. Zhang, K. E. L. Husted, S. L. Kristufek, B. Xiong, D. J. Lundberg, J. Lem, D. Veysset, Y. Sun, K. A. Nelson, D. L. Plata and J. A. Johnson, *Nature*, 2020, **583**, 542–547.
3 L. Monclús, H. P. H. Arp, K. J. Groh, A. Faltynkova, M. E. Løseth, J. Muncke, Z. Wang, R. Wolf, L. Zimmermann and M. Wagner, *Nature*, 2025, **643**, 349–355.
4 J.-B. Zhu, E. M. Watson, J. Tang and E. Y.-X. Chen, *Science*, 2018, **360**, 398–403.
5 B. A. Abel, R. L. Snyder and G. W. Coates, *Science*, 2021, **373**, 783–789.
6 P. R. Christensen, A. M. Scheuermann, K. E. Loeffler and B. A. Helms, *Nat. Chem.*, 2019, **11**, 442–448.
7 E. C. Quinn, L. J. Hamernik, J. N. Law, R. W. Clarke, M. Milrod, S. Kozarekar, R. M. Mick, M. J. Sobkowicz, L. J. Broadbelt, B. C. Knott and K. M. Knauer, *Nat. Commun.*, 2026, **17**, 1489.
8 Y. Deng, L. Liu, H.-X. Luo, H. Tian, D.-H. Qu, B. L. Feringa and Q. Zhang, *Nat. Nanotechnol.*, 2025, **20**, 1805–1812.
9 L. He, Y. Jiang, J. Wei, Z. Zhang, T. Hong, Z. Ren, J. Huang, F. Huang, P. J. Stang and S. Li, *Nat. Commun.*, 2024, **15**, 3050.
10 L. Chen, L. Yu, L. Qi, S. J. Eichhorn, A. Isogai, E. Lizundia, J. Y. Zhu and C. Chen, *Nat. Rev. Mater.*, 2025, **10**, 728–749.

11 Z. He, L. Chen, W. You, C. Zhu, X. Yang, H. Mei, D. Xiao, Q. Song, T. Shan, W. Yu, G. Li and F. Huang, *Nat. Mater.*, 2026, **25**, 107–116.
12 Z. Huang, X. Chen, S. J. K. O'Neill, G. Wu, D. J. Whitaker, J. Li, J. A. McCune and O. A. Scherman, *Nat. Mater.*, 2022, **21**, 103–109.
13 X. Yan, Z. Liu, Q. Zhang, J. Lopez, H. Wang, H.-C. Wu, S. Niu, H. Yan, S. Wang, T. Lei, J. Li, D. Qi, P. Huang, J. Huang, Y. Zhang, Y. Wang, G. Li, J. B.-H. Tok, X. Chen and Z. Bao, *J. Am. Chem. Soc.*, 2018, **140**, 5280–5289.
14 J. M. García, G. O. Jones, K. Virwani, B. D. McCloskey, D. J. Boday, G. M. Ter Huurne, H. W. Horn, D. J. Coady, A. M. Bintaleb, A. M. S. Alabdulrahman, F. Alsewailem, H. A. A. Almegren and J. L. Hedrick, *Science*, 2014, **344**, 732–735.
15 N. R. Boynton, J. M. Dennis, N. D. Dolinski, C. A. Lindberg, A. P. Kotula, G. L. Grocke, S. L. Vivod, J. L. Lenhart, S. N. Patel and S. J. Rowan, *Science*, 2024, **383**, 545–551.
16 M. Röttger, T. Domenech, R. Van Der Weegen, A. Breuillac, R. Nicolaÿ and L. Leibler, *Science*, 2017, **356**, 62–65.
17 M. J. Webber and M. W. Tibbitt, *Nat. Rev. Mater.*, 2022, **7**, 541–556.
18 S. Maes, N. Badi, J. M. Winne and F. E. Du Prez, *Nat. Rev. Chem.*, 2025, **9**, 144–158.
19 R. J. Wojtecki, M. A. Meador and S. J. Rowan, *Nat. Mater.*, 2011, **10**, 14–27.
20 J. Wang, W. Lin, V. O. Nikolaeva, R. Javaid and N. M. Khashab, *Nat. Commun.*, 2025, **16**, 7618.
21 A. W. Bosman, R. P. Sijbesma and E. W. Meijer, *Mater. Today*, 2004, **7**, 34–39.
22 Q. Zhang, V. P. Nicu, W. J. Buma, H. Tian, D.-H. Qu and B. L. Feringa, *Nat. Chem.*, 2025, **17**, 1462–1468.
23 Q. Zhang, Y.-X. Deng, H.-X. Luo, C.-Y. Shi, G. M. Geise, B. L. Feringa, H. Tian and D.-H. Qu, *J. Am. Chem. Soc.*, 2019, **141**, 12804–12814.
24 Q. Zhang, B. L. Feringa, D.-H. Qu and H. Tian, *Acc. Chem. Res.*, 2026, **59**, 151–164.
25 Z. Lei, Z. Wang, H. Jiang, J. R. Cahn, H. Chen, S. Huang, Y. Jin, X. Wang, K. Yu and W. Zhang, *Adv. Mater.*, 2024, 2407854.
26 Z. Lei, H. Chen, C. Luo, Y. Rong, Y. Hu, Y. Jin, R. Long, K. Yu and W. Zhang, *Nat. Chem.*, 2022, **14**, 1399–1404.
27 Ö. Dağlar, Y. Chen and Ž. Tomović, *Angew. Chem. Int. Ed.*, 2025, **64**, e202507567.
28 J. Demarteau, B. Cousineau, Z. Wang, B. Bose, S. Cheong, G. Lan, N. R. Baral, S. J. Teat, C. D. Scown, J. D. Keasling and B. A. Helms, *Nat. Sustain.*, 2023, **6**, 1426–1435.
29 B. A. Helms, *Acc. Chem. Res.*, 2022, **55**, 2753–2765.
30 Z. Hu, F. Hu, L. Deng, Y. Yang, Q. Xie, Z. Gao, C. Pan, Y. Jin, J. Tang, G. Yu and W. Zhang, *Angew. Chem. Int. Ed.*, 2023, **62**, e202306039.
31 W. Denissen, G. Rivero, R. Nicolaÿ, L. Leibler, J. M. Winne and F. E. Du Prez, *Adv. Funct. Mater.*, 2015, **25**, 2451–2457.
32 W. Denissen, M. Droesbeke, R. Nicolay, L. Leibler, J. M. Winne and F. E. Du Prez, *Nat. Commun.*, 2017, **8**, 14857.
33 S. Engelen, N. D. Dolinski, C. Chen, E. Ghimire, C. A. Lindberg, A. E. Crolais, N. Nitta, J. M. Winne, S. J. Rowan and F. E. Du Prez, *Angew. Chem. Int. Ed.*, 2024, **63**, e202318412.
34 M. Guerre, C. Taplan, R. Nicolaÿ, J. M. Winne and F. E. Du Prez, *J. Am. Chem. Soc.*, 2018, **140**, 13272–13284.
35 Y. Ma, X. Jiang, Z. Shi, J. A. Berrocal and C. Weder, *Angew. Chem. Int. Ed.*, 2023, **62**, e202306188.
36 X. Li, Y. Zhang, Z. Shi, D. Wang, H. Yang, Y. Zhang, H. Qin, W. Lu, J. Chen, Y. Li and G. Qing, *Nat. Commun.*, 2024, **15**, 1207.
37 X. Zhang, S. Wang, Z. Jiang, Y. Li and X. Jing, *J. Am. Chem. Soc.*, 2020, **142**, 21852–21860.

38 M. A. Rahman, C. Bowland, S. Ge, S. R. Acharya, S. Kim, V. R. Cooper, X. C. Chen, S. Irle, A. P. Sokolov, A. Savara and T. Saito, *Sci. Adv.*, 2021, **7**, eabk2451.
39 H. Lee, J. Kim, M. Lee and J. Kang, *Chem. Rev.*, 2025, **125**, 11379–11425.
40 J. Zhao, Z. Zhang, C. Wang and X. Yan, *CCS Chem.*, 2024, **6**, 41–56.
41 X. Yang, Z. Guo, L. Chen, Y. Pan, Z. He, Z. Zhang, H. Mei, N. Jiang, X. Tao, D. Xiao, G. Li and F. Huang, *J. Am. Chem. Soc.*, 2026, **148**, 6520–6530.
42 Z. Zhang, L. Cheng, J. Zhao, L. Wang, K. Liu, W. Yu and X. Yan, *Angew. Chem.*, 2020, **132**, 12237–12244.
43 J. Zhao, Z. Zhang, L. Cheng, R. Bai, D. Zhao, Y. Wang, W. Yu and X. Yan, *J. Am. Chem. Soc.*, 2021, **144**, 872–882.
44 B. Qin, S. Zhang, P. Sun, B. Tang, Z. Yin, X. Cao, Q. Chen, J. Xu and X. Zhang, *Adv. Mater.*, 2020, **32**, 2000096.
45 W. Lai, B. Qin, X. Cao, Q. Chen, J.-F. Xu and X. Zhang, *J. Am. Chem. Soc.*, 2025, **147**, 29517–29525.
46 H. Ying, Y. Zhang and J. Cheng, *Nat. Commun.*, 2014, **5**, 3218.
47 W.-X. Liu, Z. Yang, Z. Qiao, L. Zhang, N. Zhao, S. Luo and J. Xu, *Nat. Commun.*, 2019, **10**, 4753.
48 W. X. Liu, C. Zhang, H. Zhang, N. Zhao, Z. X. Yu and J. Xu, *J. Am. Chem. Soc.*, 2017, **139**, 8678–8684.
49 C. Huyan, C. Pan, Q. Chen, T. Wang, F. Yang, J. Ge, Z. Wang, D. Liu, F. Chen and L. Zhang, *Adv. Mater.*, 2026, **38**, e11620.
50 D. Liu, C. Huyan, H. Li, J. Ge, F. Chen and L. Zhang, *Adv. Mater.*, 2026, e15809.
51 E. Delebecq, J.-P. Pascault, B. Boutevin and F. Ganachaud, *Chem. Rev.*, 2013, **113**, 80–118.
52 H. Huang, W. Sun, L. Sun, L. Zhang, Y. Wang, Y. Zhang, S. Gu, Z. You and M. Zhu, *Proc. Natl. Acad. Sci. U.S.A.*, 2024, **121**, e2404726121.
53 Y. Wang, Q. Guan, Y. Guo, L. Sun, R. E. Neisiany, X. Guo, H. Huang, L. Yang and Z. You, *Sci. Adv.*, 2024, **10**, eadk5177.
54 H. Tan, L. Zhang, X. Ma, L. Sun, D. Yu and Z. You, *Nat. Commun.*, 2023, **14**, 2218.
55 B. Qian, Y. Wang, Z. Wu, Y. Jia, M. Liu, J. Su, Y. Wang, Z. Zhao, J. Wu, W. Sun, M. Tian and Z. You, *Adv. Funct. Mater.*, 2026, **36**, e09916.
56 H. Huang, L. Sun, Y. Zhang, L. Zhang, Y. Wang, W. Sun and Z. You, *Sci. Adv.*, 2026, **12**, eaea6321.
57 W. Denissen, M. Droesbeke, R. Nicolaÿ, L. Leibler, J. M. Winne and F. E. Du Prez, *Nat. Commun.*, 2017, **8**, 14857.
58 Y. Ma, X. Jiang, J. Yin, C. Weder, J. A. Berrocal and Z. Shi, *Angew. Chem. Int. Ed.*, 2023, **62**, e202212870.
59 Y. Ma, C. Zheng, G. Slor, M. Özkan, O. J. Gubelmann and F. Stellacci, *Angew. Chem. Int. Ed.*, 2024, **63**, e202410624.
60 Y. Ma, C. Zheng, D. Raphaël Bréas, G. Slor, A. P. A. Molleyres, Q. Liao and F. Stellacci, *Angew. Chem. Int. Ed.*, 2025, **64**, e202516735.
61 Y. Ma, C. Weder, F. E. Du Prez and J. A. Berrocal, *Chem. Rev.*, 2025, **125**, 9296–9331.
62 Y. Ma, J. A. Berrocal, X. Jiang and Z. Shi, *ACS Sustain. Chem. Eng.*, 2023, **11**, 7917–7923.
63 Z. Liu and Y. Ma, *ChemSusChem*, 2025, **18**, e202500436.
64 W. Liu, S. Yang, L. Huang, J. Xu and N. Zhao, *Chem. Commun.*, 2022, **58**, 12399–12417.
65 C. Zheng, G. Slor, Y. Ma and F. Stellacci, *ACS Macro Lett.*, 2024, **13**, 1704–1710.
66 G. Slor, Y. Ma, H. Park, T. Choi, D. Guironnet and F. Stellacci, *Adv. Funct. Mater.*, 2025, e18059.
67 S. Kim, L. M. Felsenthal, O. Sala, O. Welz, M. Bergeler, A. Alsbaiee and W. R. Dichtel, *J. Am. Chem. Soc.*, 2025, **147**, 35655–35663.

68 P. N. Swathi, H. June, J. Kim, V. Murali, C. H. Tran, W. S. Kim, J. W. Han and J. Jae, *Angew. Chem. Int. Ed.*, 2025, **65**, e15043.
69 R. Villa, R. Salas, M. Maciá, F. Velasco, B. Altava, E. García-Verdugo and P. Lozano, *Angew. Chem. Int. Ed.*, 2025, **64**, e202418034.
70 H. Feng, N. Zheng, W. Peng, C. Ni, H. Song, Q. Zhao and T. Xie, *Nat. Commun.*, 2022, **13**, 397.
71 Z. Liu, Z. Fang, N. Zheng, K. Yang, Z. Sun, S. Li, W. Li, J. Wu and T. Xie, *Nat. Chem.*, 2023, **15**, 1773–1779.
72 Z. Liu, L. Liu, Y. Li, K. Yang, S. Li, W. Li, Y. Zhu and T. Xie, *Nat. Commun.*, 2025, **16**, 5117.
73 X. Zhang, X. Pu, L. Xia, W. Peng, Y. Ji, J. Xu, J. Wu, L. Jiang, Q. Zhao, Z. Fang and T. Xie, *Natl. Sci. Rev.*, 2025, **12**, nwaf501.
74 S. Yang, S. Du, J. Zhu and S. Ma, *Chem. Soc. Rev.*, 2024, **53**, 9609–9651.
75 L. T. J. Korley, T. H. Epps, B. A. Helms and A. J. Ryan, *Science*, 2021, **373**, 66–69.
76 P. Yu, Q. Huang, Y. Wang, W. Peng, Z. Jia, H. Wang, J. Ma, C. Wang and X. Yan, *Chin. J. Chem.*, 2024, **42**, 516–522.
77 P. Li, X. Jiang, R. Gu, H. Tian and D.-H. Qu, *Angew. Chem. Int. Ed.*, 2024, **63**, e202406708.
78 P. Li, J. Zhang, Z. Wang, C. Li, H. Wu, M. Lei, G. Yan, H. Tian, R. Gu and D. Qu, *Angew. Chem. Int. Ed.*, 2025, **64**, e202506939.
79 S. Wang, H. Feng, B. Li, J. Y. C. Lim, W. Rusli, J. Zhu, N. Hadjichristidis and Z. Li, *J. Am. Chem. Soc.*, 2024, **146**, 16112–16118.
80 S. Wang, H. Feng, J. Y. C. Lim, K. Li, B. Li, J. J. Q. Mah, Z. Xing, J. Zhu, X. J. Loh and Z. Li, *J. Am. Chem. Soc.*, 2024, **146**, 9920–9927.
81 L. Pettazzoni, M. Ximenis, F. Leonelli, G. Vozzolo, E. Bodo, F. Elizalde and H. Sardon, *Chem. Sci.*, 2024, **15**, 2359–2364.
82 D. Roca-López, A. Darù, T. Tejero and P. Merino, *RSC Adv.*, 2016, **6**, 22161–22173.

View Article Online
DOI: 10.1039/D6SC04529D

The data supporting this article have been included as part of the supplementary information (SI). Supplementary information: materials, experimental procedures, characterizations, theoretical calculations, SI Figure S1–S45.